Journal of Materials Science: Materials in Electronics (2020) 31:12137–12147
https://doi.org/10.1007/s10854-020-03760-6

Novel AgCl nanoparticles coupling with $PbBiO_2Br$ nanosheets for green and efficient degradation of antibiotic oxytetracycline hydrochloride under visible-light irradiation

Wen Li[1,2] · Zhiying Liu[3] · Wei Song[4] · Yanhua Xu[3]

Received: 18 March 2020 / Accepted: 7 June 2020 / Published online: 17 June 2020

Abstract
In this work, novel Ag/AgCl/$PbBiO_2Br$ photocatalysts were synthesized via a hydrothermal and in situ photoreaction method. The microstructure, morphology, composition, electrochemical, and optical properties of the synthesized catalysts were investigated by multiple techniques. The obtained Ag/AgCl, $PbBiO_2Br$, and Ag/AgCl/$PbBiO_2Br$ composites were evaluated via degradation of oxytetracycline (OTC) hydrochloride antibiotic under visible-light irradiation. The results show that the Ag/AgCl/$PbBiO_2Br$ composites are composed of Ag/AgCl nanoparticles (NPs) and $PbBiO_2Br$ nanosheets. The Ag/AgCl/$PbBiO_2Br$ (20.4%) composite exhibits the highest visible-light absorption and best photogenerated charge separation efficiency. The photocatalytic degradation experiments show that all Ag/AgCl/$PbBiO_2Br$ composites exhibit an enhanced degradation activity under visible-light irradiation, and maintain good stability in the photocatalytic process. The Ag/AgCl/$PbBiO_2Br$ (20.4%) composite has the highest degradation activity, which is 1.82 and 2.11 times higher than that of Ag/AgCl and $PbBiO_2Br$, respectively. The enhanced photocatalytic activity of Ag/AgCl/$PbBiO_2Br$ can be mainly attributed to the fact that the loading of Ag NPs on the surface of the AgCl promotes the separation efficiency of photoinduced charge and enhance the visible-light absorption. Additionally, active species trapping experiments confirm that superoxide radicals ($\cdot O_2^-$), Cl^0 and holes (h^+) play an very important role in the degradation process.

1 Introduction

Nowadays, the widespread usage of antibiotics has received the increasing attention because they flow into the water system and cause the water pollution [1]. Oxytetracycline (OTC) hydrochloride is one of the very important antibiotics, extensively used in human and veterinary medicine [2]. Worryingly, the most of OTC is only partially metabolized in humans or animals and hardly biologically degraded, ultimately released into lakes and rivers. These antibiotics have harmful effects on water environment and human health [3]. Hence numbers of research attempts have been made in the past decades to eliminate these refractory antibiotics, such as electrochemical treatments [4], photoelectron-Fenton [5] and advanced oxidation treatment [6]. However, most of the methods use expensive oxidants. Therefore, it is indispensable to develop novel visible-light-driven photocatalysts [7], which are environmentally friendly and efficient approach to remove OTC from waters.

$PbBiO_2Br$ is an n-type visible-light-driven semiconductor and has attracted more and more attention in recent years, owing to its physicochemical stability, highly anisotropic layered structure, and outstanding photocatalytic performance [8–11]. Unfortunately, the photocatalytic activity of bare $PbBiO_2Br$ is still unsatisfactory owing to its fast recombination rate of photoexcited electron–hole (e^-/h^+) pairs [12, 13]. To overcome the above mentioned drawback of $PbBiO_2Br$ and improve the degradation efficiency, constructing semiconductor composites is effective

Electronic supplementary material The online version of this article (https://doi.org/10.1007/s10854-020-03760-6) contains supplementary material, which is available to authorized users.

✉ Yanhua Xu
lw_water@126.com

1 College of Civil Engineering, Nanjing Tech University, Nanjing 211816, China

2 School of Environmental & Safety Engineering, Changzhou University, Changzhou 213164, Jiangsu, China

3 School of Environmental Science and Engineering, Nanjing Tech University, Nanjing 211816, China

4 Changzhou Zhiheng Environmental Technology Co., Ltd, Changzhou 213164, Jiangsu, China

in improving the separation efficiency of photoinduced e^-/h^+ pairs. So far, studies have reported on g-C_3N_4/$PbBiO_2Br$ [14], $NbSe_2$/$PbBiO_2Br$ [15], $PbBiO_2Br$/UiO-66-NH_2 [16] Cu_2O/$PbBiO_2Br$ [17], *p*-Ag_2O/*n*-$PbBiO_2Br$ [18], $PbBiO_2Br$/BiOBr composites [19], and etc. These heterojunction composites were found to exhibit superior photocatalytic activity. Despite many $PbBiO_2Br$-based materials have been reported, it is still necessary to be committed to the exploitation of more efficient visible-light-driven $PbBiO_2Br$-based photocatalysts for making the best use of the solar energies.

The surface plasmon resonance (SPR) strategy is widely used in fabricating efficient visible-light-driven photocatalysts [20]. Because of SPR of noble metal nanoparticles (NPs), the absorption range of visible-light region can be expanded, resulting in the enhanced degradation performance of photocatalysts [21]. Recently, Ag/AgCl has been widely considered as a promising photocatalyst due to its being a p-type SPR structure semiconductor [22]. Furthermore, Ag^0 NPs dispersed on the surface of AgCl can not only effectively absorb visible light, but also can accelerate the transfer of photo-carriers. By now, a number of Ag/AgCl-based photocatalysts have been successfully synthesized, such as Ag/AgCl/$NaTaO_3$ [23], and $BiVO_4$/MWCNT/Ag@AgCl [24]. These composite photocatalysts exhibited superior photocatalytic performances. To the best of our knowledge, the coupling of $PbBiO_2Br$ nanosheets with Ag/AgCl NPs has not been reported yet. Hence, we expect that the new Ag/AgCl/$PbBiO_2Br$ composites not only improve the utilization rate of solar energy, but also enhance photocatalytic ability.

Inspired by previous studies, we have successfully fabricated a series of Ag/AgCl/$PbBiO_2Br$ composites by a hydrothermal and in situ photoreaction method. Morphology and microstructure, elements chemical states, optical and electrochemical properties of the Ag/AgCl/$PbBiO_2Br$ composites were systematically studied. Their photocatalytic performances were investigated by the degradation of OTC under visible-light irradiation. The possible enhanced photocatalytic mechanism was also proposed.

2 Experimental

2.1 Preparation of the photocatalysts

$PbBiO_2Br$ nanosheets were synthesized via a facile hydrothermal method [17]. Detailed experimental process was given in Supporting Information (S1). Ag/AgCl/$PbBiO_2Br$ composites were prepared via a photoreduction method. The preparation process was as follows: 1 mmol of $PbBiO_2Br$ was dispersed in deionized water, stirred for 20 min to form uniform suspension A. Then, 1 mmol $AgNO_3$ was added into the suspension A and stirred for 20 min. Subsequently, 1 mmol NaCl was transferred into the suspension A under strong stirring for 30 min. The resulting mixture was illuminated under a 500 W xenon lamp for 30 min so that the Ag^+ NPs on the surface of AgCl/$PbBiO_2Br$ were reduced to Ag^0 NPs. Eventually, the precipitate was filtered, rinsed with deionized water and ethanol, and dried at 80 °C for 24 h. The obtained product, in which the mass ratio of Ag to $PbBiO_2Br$ was 20.4%, was designated as Ag/AgCl/$PbBiO_2Br$ (20.4%). Ag/AgCl/$PbBiO_2Br$ (13.6%), Ag/AgCl/$PbBiO_2Br$ (40.8%), and bare Ag/AgCl were also obtained with the same conditions by changing the content of $PbBiO_2Br$.

2.2 Characterization and photocatalytic evaluation

The synthesized catalysts were investigated in detail by multiple instruments analyses. The photocatalytic activities of the Ag/AgCl, $PbBiO_2Br$, and Ag/AgCl/$PbBiO_2Br$ composites were evaluated via the degradation of the antibiotic OTC under visible-light irradiation. Detailed experimental process was given in Supporting Information (S2).

2.3 Photoelectrochemical measurements

The electrochemical properties of as-prepared samples were investigated on a electrochemical workstation (CS350H, wuhan sikete instrument Co., Ltd, China) with standard calomel electrode (SCE). Preparation of the working electrodes and detailed experimental process were given in Supporting Information (S3).

3 Results and discussion

3.1 XRD analysis

The crystal structures of as-synthesized $PbBiO_2Br$, Ag/AgCl, and Ag/AgCl/$PbBiO_2Br$ (20.4%) composite were analyzed using X-ray diffraction (XRD), as presented in Fig. 1a. It can be seen that the XRD pattern of bare $PbBiO_2Br$ was consistent with the standard spectrum of tetragonal phase $PbBiO_2Br$ (PDF#38-1008). The strong peak located at 30.6° corresponds to the (103) plane of $PbBiO_2Br$, indicating that the obtained catalyst is well-crystallized [25]. For the Ag/AgCl, the peaks at $2\theta = 27.7°$, 32.1°, 46.1°, 54.7°, and 57.3°correspond to the (111), (200), (220), (311), and (222) planes of cubic AgCl (PDF#31-1238), respectively [26]. In addition, the diffraction peaks at $2\theta = 37.9°$, 44.1°, 64.3°, and 77.2° match with the (111), (200), (220), and (311) facets of Ag crystal (PDF# 65-2871), respectively [27]. Additionally, as for the Ag/AgCl/$PbBiO_2Br$ (20.4%) photocatalyst, all the diffraction peaks correspond to $PbBiO_2Br$ and Ag/AgCl, and no additional crystal phases can be detected, which indicates the formation of Ag/AgCl/$PbBiO_2B$ composites.

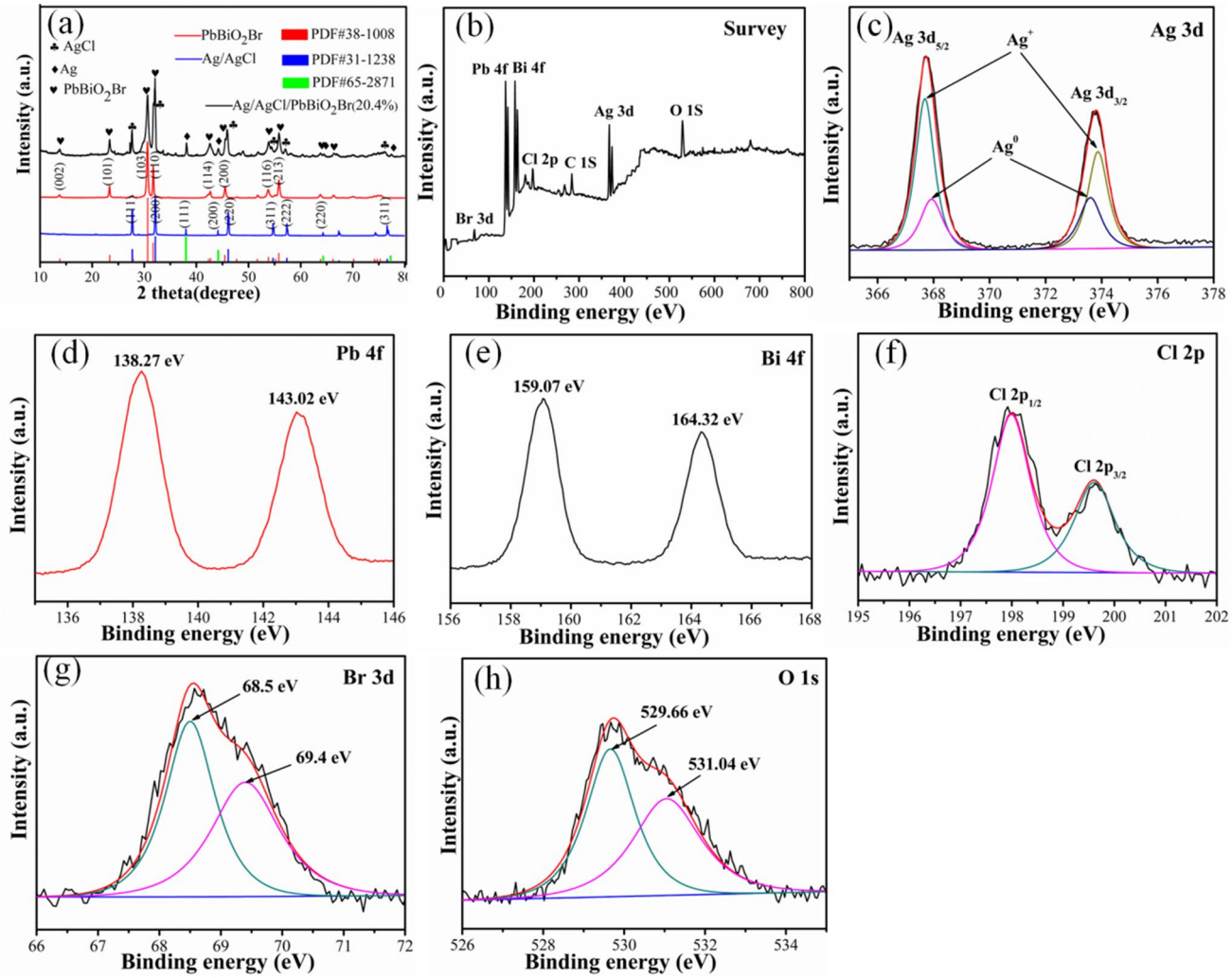

Fig. 1 **a** XRD patterns of Ag/AgCl, $PbBiO_2Br$, and Ag/AgCl/$PbBiO_2Br$ (20.4%) composite. XPS spectra of Ag/AgCl/$PbBiO_2Br$ (20.4%) composite; **b** the XPS survey spectrum, **c** Ag 3d, **d** Pb 4f, **e** Bi 4f, **f** Cl 2p, **g** Br 3d and **h** O 1s

3.2 XPS analysis

The elemental valence states of the as-synthesized Ag/AgCl/$PbBiO_2Br$ (20.4%) were detected by X-ray photoelectron spectroscopy (XPS) technology, and the obtained results are illustrated in Fig 1. The main peaks in the XPS survey spectrum of Ag/AgCl/$PbBiO_2Br$ (20.4%) composite (Fig 1b) correspond to Br 3d, Pb 4f, Bi 4f, Cl 2p, Ag 3d, and O 1s. Figure 1c displays the XPS spectrum of Ag 3d, where the peaks at 367.93 and 373.60 eV are assigned to Ag^0, and the other two strong peaks at 367.69 and 373.87 eV are ascribed to Ag $3d_{5/2}$ and Ag $3d_{3/2}$ of Ag^+ in Ag/AgCl, respectively. This result is consistent with other reports in literatures [28]. In Fig. 1d, the binding energy peaks at 138.27 and 143.02 eV are corresponding to Pb $4f_{7/2}$ and Pb $4f_{5/2}$, respectively [29]. Figure 1e shows that the XPS spectrum of Bi element, where the peaks at 157.09 and 164.32 eV are attributed to Bi $4f_{7/2}$ and Bi $4f_{5/2}$, respectively [30–34], indicating that Bi^{3+} ions exist in $PbBiO_2Br$. Furthermore, in Fig 1f, two typical peaks at 199.61 and 197.99 eV can be attributed to Cl $2p_{3/2}$ and Cl $2p_{1/2}$, indicating that Cl^- ions exist in AgCl phase [34]. Figure 1g shows the XPS spectrum of Br 3d, where the binding energy peaks at 68.5 and 69.4 eV are corresponding to Br $3d_{3/2}$ and Br $3d_{5/2}$, respectively [35]. The O 1s XPS spectrum of Ag/AgCl/$PbBiO_2Br$ (20.4%) composite (Fig. 1h) is composed of fitted peaks at 529.66 and 531.04 eV, which could be attributed to the lattice oxygen of $PbBiO_2Br$ and surface-adsorbed oxygen species, respectively [36, 37]. From the XPS analysis, it is clear that Ag/AgCl/$PbBiO_2Br$ is a composite sample composed of Ag/AgCl and $PbBiO_2Br$.

3.3 Scanning electron microscope (SEM) and EDX analysis

Figure 2 shows the morphologies of the $PbBiO_2Br$, Ag/AgCl, and Ag/AgCl/$PbBiO_2Br$ (20.4%) composite. Figure 2a reveals that the AgCl consists of cubic-like NPs with grain size of 300–500 nm and Ag NPs are dispersed on the surfaces of AgCl cubes. Figure 2b shows that the as-prepared $PbBiO_2Br$ has a sheet-like morphology with thickness about 30 nm. As seen from Fig. 2c, the Ag/AgCl NPs are attached on the surface of $PbBiO_2Br$ nanosheets. Moreover, we also notice that compared with the pure Ag/AgCl, the particle size of Ag/AgCl in the Ag/AgCl/$PbBiO_2Br$ (20.4%) composite undergoes significant change, which could be due to the fact that $PbBiO_2Br$ could influence the surface energy of Ag/AgCl and thus impede their growth. Additionally, energy-disperse X-ray (EDX) spectroscopy analysis of Ag/AgCl/$PbBiO_2Br$ (20.4%) composite was carried out, and the obtained result is illustrated in Fig. 2d. From the EDX spectrum, the peaks belonging to Ag, Cl, Pb, Bi, O, C, Au, and Br are observed (C and Au element come from the test instrument). The atomic ratio of Ag/Pb equals to 1:1, which is in good agreement with the Ag/Pb atomic ratio of Ag/AgCl/$PbBiO_2Br$ (20.4%) composite.

3.4 TEM analysis

To further obtain more detailed structure information of Ag/AgCl/$PbBiO_2Br$ (20.4%) composite, field emission transmission electron microscopy (TEM) and high resolution TEM (HRTEM) images were carried out. As shown in Fig. 2e, the Ag/AgCl NPs are formed on the surface of $PbBiO_2Br$ nanosheets. From Fig. 2f, it is clearly seen that the lattice fringes of 0.235 and 0.277 nm are corresponding to the (111)

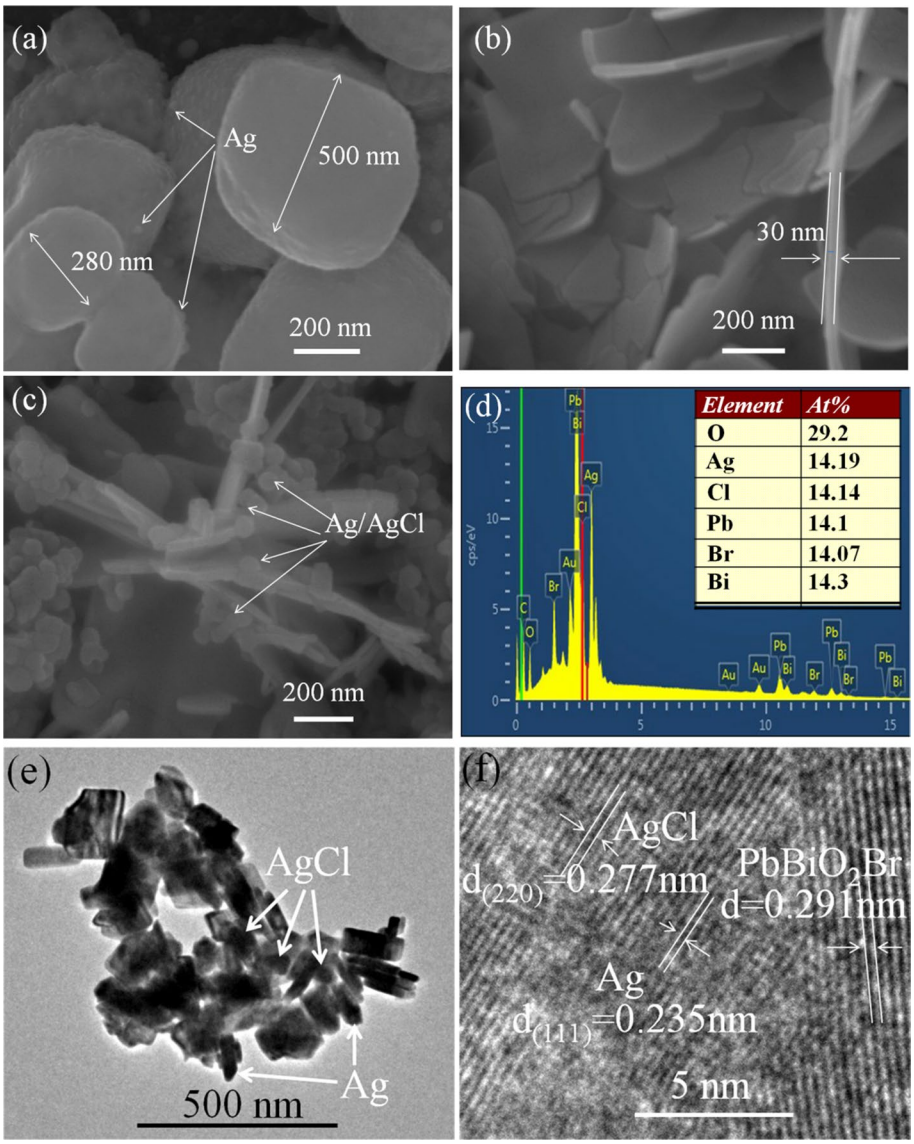

Fig. 2 SEM images of **a** Ag/AgCl, **b** $PbBiO_2Br$, and **c** Ag/AgCl/$PbBiO_2Br$ (20.4%); **d** EDS spectrum, **e** TEM and **f** HRTEM images of as-prepared Ag/AgCl/$PbBiO_2Br$ (20.4%) composite

and (220) planes of Ag and AgCl, respectively [38]. The lattice fringes of 0.291 nm are correlated with the (103) plane of $PbBiO_2Br$ [39].

3.5 Optical properties of the photocatalysts

The optical properties of photocatalysts are very important for their photocatalytic application in the degradation of the antibiotics. Therefore, the optical properties of as-obtained bare $PbBiO_2Br$, Ag/AgCl, and different Ag/AgCl/$PbBiO_2Br$ composites were investigated via ultraviolet–visible diffuse reflectance spectra (UV–Vis DRS) measurement, as shown in Fig. 3a. The bare $PbBiO_2Br$ exhibits the absorption edge at 500 nm, which is in agreement with the previous results in literatures [17, 40]. It can be seen that Ag/AgCl exhibits a strong absorption in the visible-light region. It is also obvious that the absorption intensities of Ag/AgCl/$PbBiO_2Br$ composites are stronger than that of bare $PbBiO_2Br$ in the visible-light regions, which can be attributed to the Ag SPR strategy [41].

3.6 FT-IR analysis

Figure 3b shows the Fourier transform infrared spectroscopy (FT-IR) spectra of the samples. For the pristine Ag/AgCl sample, the peak at 1044.1 cm^{-1} is attributed to the stretching vibration of Ag–Cl [42]. Furthermore, the stretching vibration of Ag NPs bond can be also observed at 2790.1 and 2908.7 cm^{-1} [43]. For pure $PbBiO_2Br$, the peaks at 1388.4 and 1600.1 cm^{-1} are attributed to the bending vibrations of the Pb–O bond and the Bi–O bond, respectively [44, 45]. The broad absorption bands on the right side from 3250 to 3425 cm^{-1} are corresponding to the stretching vibration O–H band by the absorbed H_2O [46, 47]. As for the Ag/AgCl/$PbBiO_2Br$ composites, all the absorption peaks are from Ag/AgCl and $PbBiO_2Br$. The analysis results indicate that Ag/AgCl/$PbBiO_2Br$ are successfully fabricated.

3.7 Nitrogen adsorption analysis

According to the previously reported literature [47–49], the photocatalytic efficiency of the catalyst is largely dependent on its specific surface area, so the Brunauer–Emmett–Teller (BET) specific surface areas of the as-prepared samples were measured using nitrogen adsorption–desorption measurements. The BET specific surface areas of pure $PbBiO_2Br$, Ag/AgCl, and Ag/AgCl/$PbBiO_2Br$ composites are summarized in Table 1. It is found that the BET specific surface area of the Ag/AgCl/$PbBiO_2Br$ (20.4%) is measured to be 37.16 m^2/g, which is 3.06 times higher than that of pure $PbBiO_2Br$ (12.12 m^2/g). The much larger surface area facilitates the contaminant contact with the catalyst and enhances the photocatalytic performance.

3.8 Photocatalytic activity

The removal of OTC was used to evaluate the photocatalytic properties of the obtained photocatalysts under visible-light irradiation, and the attained results are given in Fig. 4a. No apparent OTC degradation is detected without photocatalyst under visible-light irradiation, indicating that the direct

Table 1 BET specific surface areas of the as-prepared samples

Samples	BET(m^2/g)
Pure $PbBiO_2Br$	12.12
Ag/AgCl/$PbBiO_2Br$ (13.6%)	25.82
Ag/AgCl/$PbBiO_2Br$ (20.4%)	37.16
Ag/AgCl/$PbBiO_2Br$ (40.8%)	32.01
Ag/AgCl	26.14

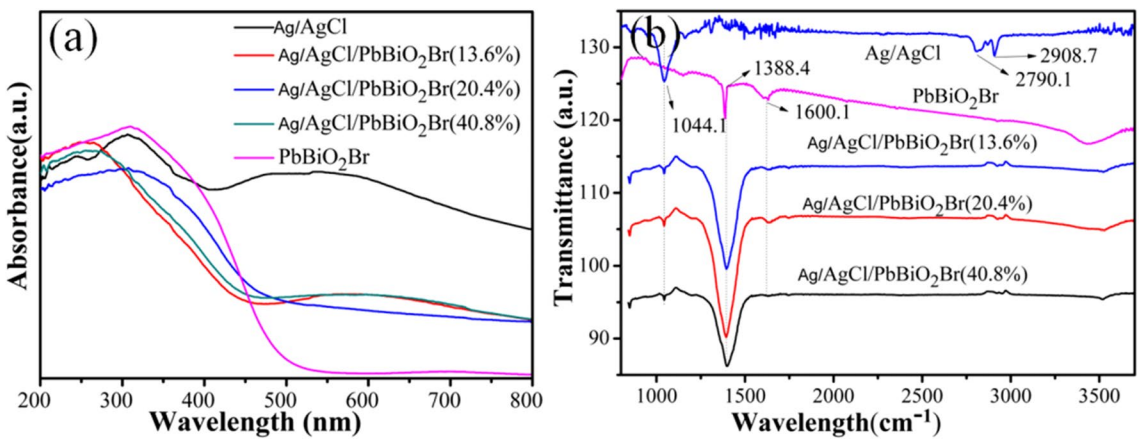

Fig. 3 **a** UV–Vis absorption spectra and **b** FT-IR spectra of bare $PbBiO_2Br$, Ag/AgCl and different Ag/AgCl/$PbBiO_2Br$ composites

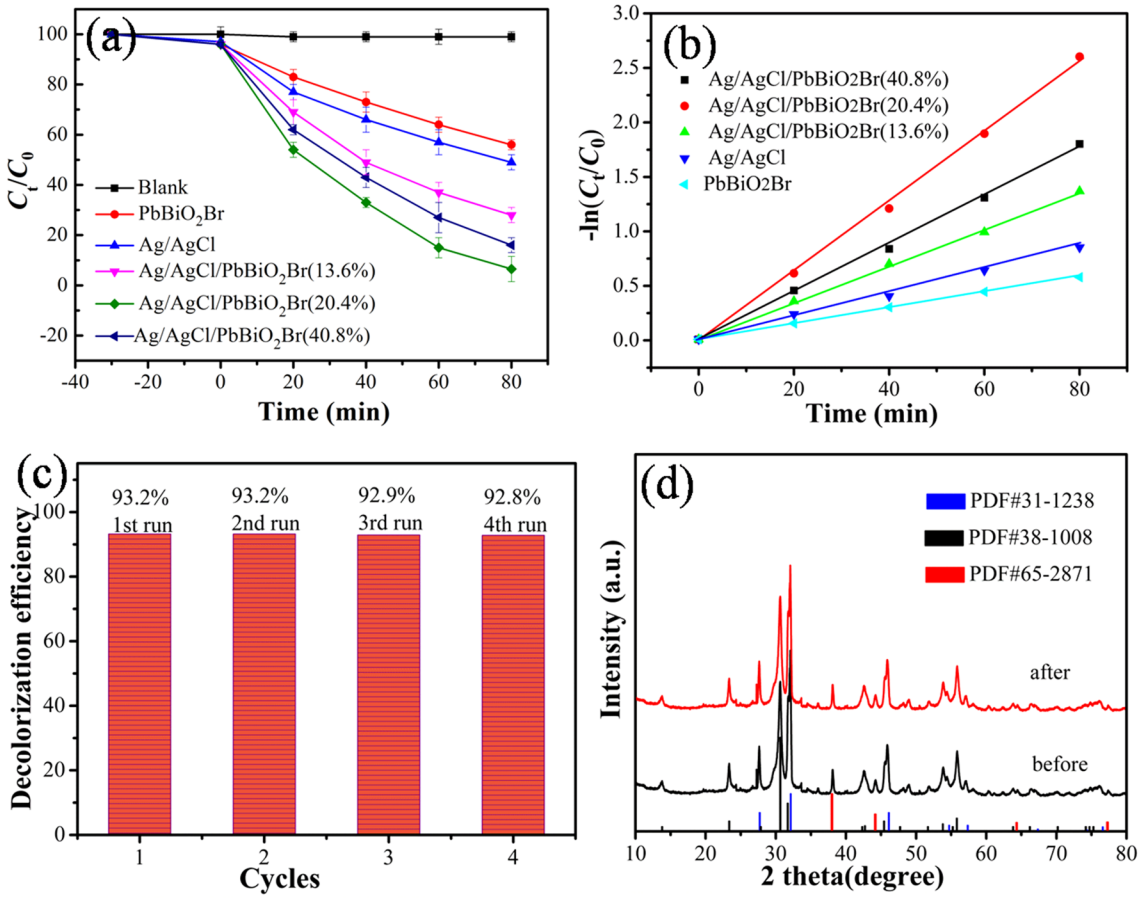

Fig. 4 **a** OTC photodegradation and **b** $-\ln(C_t/C_0)$ vs. time plots for photodegradation of OTC by the obtained catalysts; **c** Cycling degradation efficiency of Ag/AgCl/$PbBiO_2Br$ (20.4%) composite and **d** XRD patterns of Ag/AgCl/$PbBiO_2Br$ (20.4%) composite before and after the recycling photocatalytic experiment

photolysis of OTC can be almost neglected. It can be observed that 44% and 51% of OTC solution is removed within 80 min visible-light irradiation for bare $PbBiO_2Br$ and Ag/AgCl, respectively. However, the Ag/AgCl/$PbBiO_2Br$ composites exhibit enhanced photocatalytic activity in comparison to pure $PbBiO_2Br$ and Ag/AgCl under identical experimental conditions. The degradation percentage of OTC solution reaches 72%, 93.2%, and 84% for Ag/AgCl/$PbBiO_2Br$ (13.6%), Ag/AgCl/$PbBiO_2Br$ (20.4%), and Ag/AgCl/$PbBiO_2Br$ (40.8%) composites within 80 min visible-light irradiation, respectively. It is worth noting that the Ag/AgCl/$PbBiO_2Br$ (40.8%) photocatalyst has a higher mass ratio of Ag than the Ag/AgCl/$PbBiO_2Br$ (20.4%) photocatalyst, however, the photocatalytic activity of the former is lower than that of the latter. The reason may be that Ag NPs are loaded on the surface of the photocatalyst, which not only motivate the SPR, but also promote separation of electrons and holes. However, excessive Ag NPs covering on surface of the AgCl could inhibit the light absorption and decrease the separation efficiency of e^-/h^+ pairs, thus leading to decreased photocatalytic activity. In addition, to get further insight into the reaction kinetic behaviors, the photocatalytic degradation rates are calculated using the following equation [50–52]:

$$\ln\left(C_t/C_0\right) = K_{app}t \quad (1)$$

where, k_{app} stands for degradation rates constant [53]. The results are drawn and displayed in Fig. 4b. The obtained rate constants k_{app} are 1.06×10^{-2}, 7.25×10^{-3}, 1.71×10^{-2}, 3.25×10^{-1} and 2.21×10^{-1} min^{-1} for Ag/AgCl, $PbBiO_2Br$, Ag/AgCl/$PbBiO_2Br$ (13.6%), Ag/AgCl/$PbBiO_2Br$ (20.4%), and Ag/AgCl/$PbBiO_2Br$(40.8%), respectively. It is clear that the rate constant k_{app} of Ag/AgCl/$PbBiO_2Br$ (20.4%) is 3.04 and 4.48 times higher than that of Ag/AgCl and $PbBiO_2Br$, respectively. These results confirm that Ag/AgCl/$PbBiO_2Br$ composites accelerate the degradation of OTC in photocatalytic progress.

3.9 Cyclic experiments

In order to investigate the structural stability and practical application of Ag/AgCl/$PbBiO_2Br$ (20.4%) composite,

recycling experiments were performed under the same condition, as shown in Fig. 4c. It can be observed that after the 4th run recycle experiment, the removal efficiency of Ag/AgCl/$PbBiO_2Br$ (20.4%) photocatalyst decreases from 93.2 to 92.8%. This implies that the decrease of the degradation efficiency can be negligible. Furthermore, Fig. 4d exhibits the XRD patterns of Ag/AgCl/$PbBiO_2Br$ (20.4%) photocatalyst before and after photodegradation recycling. It is clearly observed that all diffraction peaks undergo no change, indicating no any change in crystalline structure. Above results further confirm the stability of the Ag/AgCl/$PbBiO_2Br$ composites during photocatalytic process.

3.10 Possible photocatalytic mechanism

As we all know, superoxide radicals ($\cdot O_2^-$), hydroxyl radicals (·OH) and holes (h^+) are involved in the photocatalytic reaction system as the main radical species [54]. To explore the role of the active species, the radical trapping experiments was implemented by separately adding 10 mM ethylene diaminetetraacetic acid disodium salt (EDTA-2Na), 10 mM isopropanol (IPA) and 1 mM benzoquinone (BQ) into the photocatalytic reaction system, which act as the h^+, ·OH and $\cdot O_2^-$ scavengers, respectively. As depicted in Fig. 5, it is evident that with adding IPA, the degradation rate of Ag/AgCl/$PbBiO_2Br$ (20.4%) decreases slightly to 90.5%, demonstrating that there are almost no ·OH radicals generated in the degradation process. However, when adding BQ or EDTA-2Na, the degradation efficiency sharply decreases from 93.2 to 17 and 26%, respectively, demonstrating that $\cdot O_2^-$ and h^+ play very important role in the degradation process. Furthermore, in this study, considering that the Cl^- could be oxidized by holes to Cl^0 atoms and the antibiotics OTC could be oxidized [55]. Cl^0 atoms are considered to be another actual active species in the photocatalytic degradation process [56].

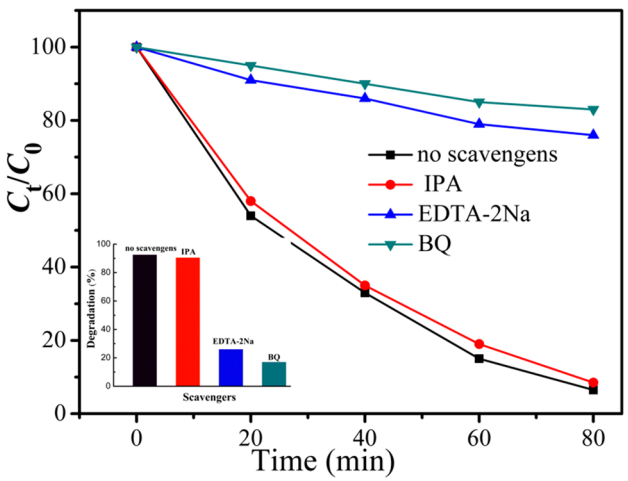

Fig.5 The degradation of OTC on the Ag/AgCl/$PbBiO_2Br$ (20.4%) composite in presence of various scavengers

Many researches indicate that photoluminescence (PL) emission spectra can be induced by the recombination between photogenerated electrons and holes [57]. The lower the PL emission peaks, the less the recombination of photoexcited charge carriers. Therefore, the charge transfer and recombination processes in the photodegradation experiment can be investigated by PL spectra. Figure 6a shows the PL spectra of bare $PbBiO_2Br$, Ag/AgCl, and different Ag/AgCl/$PbBiO_2Br$ composites in the range of 420–620 nm under excitation at 325 nm, which arise due to the recombination of photogenerated electrons and holes. It is observed that the emission spectrum intensity of bare $PbBiO_2Br$ is the strongest. However, after the coupling of Ag/AgCl NPs with $PbBiO_2Br$ nanosheets, the intensity of the PL emission spectra is decreased, indicating that the charge separation rate of Ag/AgCl/$PbBiO_2Br$ composites is more efficient than that of bare $PbBiO_2Br$ and Ag/AgCl nanoplates. It is noteworthy that the Ag/AgCl/$PbBiO_2Br$ (20.4%) composite exhibits the weakest intensity, suggesting that it has the highest separation efficiency of photoexcited charge carriers [58]. In order to further understand the charge transfer in the photocatalytic process. Electrochemical impedance spectroscopy (EIS) measurement was also carried out for the bare $PbBiO_2Br$, Ag/AgCl, and Ag/AgCl/$PbBiO_2Br$ (20.4%) composite. As shown in Fig. 6b, it is found that Ag/AgCl/$PbBiO_2Br$ (20.4%) composite owns the smallest semicircle

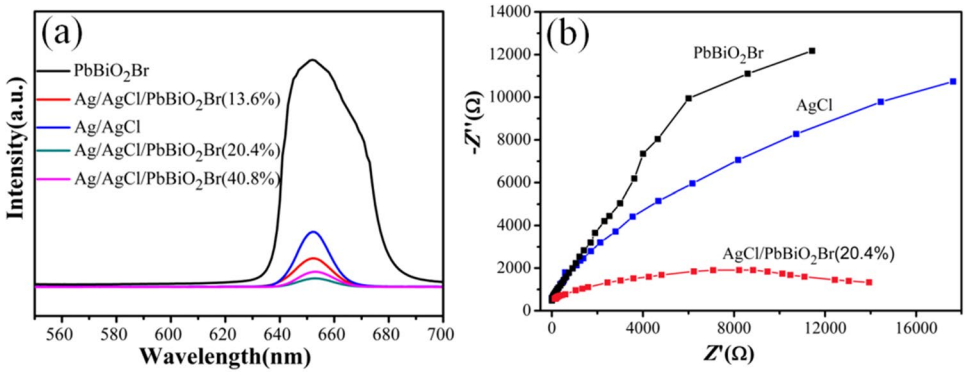

Fig. 6 **a** PL spectra (excited at 325 nm) and **b** EIS Nyquist plots of the as-synthesized samples

radius. It is commonly recognized that the curvature radius serves as an indicator of charge-transfer resistance, and a smaller semicircle radius implies higher charge transfer efficiency [59, 60].

The positions of the conduction band (CB) and valence band (VB) of obtained $PbBiO_2Br$ are about − 1.0 and 1.5 eV (vs.NHE), respectively, according to our previously reported results [17, 18]. Furthermore, in the light of the literature, the positions of the CB and VB of the AgCl are located at − 0.09 and 3.16 eV (vs. NHE), respectively [23, 25].

In the light of above experimental results, a possible photocatalysis mechanism is proposed to explain the charge transfer behaviors of $Ag/AgCl/PbBiO_2Br$ composite in the photocatalytic process. As shown in Fig. 7, the $PbBiO_2Br$ and metallic Ag NPs are photoexcited to generate e^-/h^+ under visible-light irradiation (Eqs. 2, 3). The AgCl is difficult to be stimulated under visible-light irradiation due to its broad bandgap. Since the SPR of Ag NPs is energetic enough to the photoexcited electrons and can be easily injected into the E_{CB} of AgCl or $PbBiO_2Br$ (Eq. 4). These accumulated electrons on the E_{CB} of AgCl could not reduce oxygen to form $\cdot O_2^-$, due to the E_{CB} potential of AgCl (− 0.09 eV) more positive than the standard reduction potential of $E_0\left(O_2/\cdot O_2^-\right) = -0.33$ eV vs. NHE [61–64]. These accumulated charges could react with O_2 on the surface of $PbBiO_2Br$ to form $\cdot O_2^-$ due to the E_{CB} potential of $PbBiO_2Br$ (− 1.0 eV) more negative than the standard reduction potential of $E_0\left(O_2/\cdot O_2^-\right) = -0.33$ eV vs. NHE (Eq. 5). Above radical trapping experimental results verify that the $\cdot O_2^-$ is one of the main active species in the photocatalytic process. Meanwhile, the residual h^+ at Ag NPs migrates to the E_{VB} of AgCl surface to oxidize the Cl^- ion to form Cl^0 atoms (Eqs. 6, 7). The Cl^0 atoms are reactive radical species. After that, Cl^0 atoms oxidize OTC and hence are reduced to Cl^- again (Eq. 8) [65, 66]. Thus, the $Ag/AgCl/PbBiO_2Br$ can maintain good catalytic performance and stability. On the other hand, from a thermodynamic point of view, the photogenerated h^+ cannot react with OH^- or H_2O to produce ·OH since the VB potential of $PbBiO_2Br$ is more negative than the redox potentials of $E^0(OH^-/\cdot OH)$ (1.99 eV vs. NHE) and $E^0\left(H_2O/\cdot OH\right)$ (2.38 eV vs. NHE), indicating that the h^+ can directly oxide OTC [67–69]. The produced active species (h^+,$\cdot O_2^-$) can efficiently decompose OTC into intermediate products and finally into H_2O and CO_2 (Eq. 9). The above discussion suggests that the $Ag/AgCl/PbBiO_2Br$ composites can improve the separation of photogenerated e^-/h^+, finally leading to the enhancement of photocatalytic activity.

$$Ag + h\nu \rightarrow Ag(e^-)_{CB} + Ag\left(h^+\right)_{VB} \tag{2}$$

$$PbBiO_2Br + h\nu \rightarrow PbBiO_2Br(e^-)_{CB} + PbBiO_2Br\left(h^+\right)_{VB} \tag{3}$$

$$Ag(e^-)_{CB} + PbBiO_2Br \rightarrow PbBiO_2Br(e^-)_{CB} + Ag \tag{4}$$

$$PbBiO_2Br(e^-)_{CB} + O_2 \rightarrow \cdot O_2^- \tag{5}$$

$$Ag\left(h^+\right)_{VB} + AgCl \rightarrow AgCl\left(h^+\right)_{VB} + Ag \tag{6}$$

$$AgCl\left(h^+\right)_{VB} + Cl^- \rightarrow Cl^0 + AgCl \tag{7}$$

$$Cl^0 + OTC \rightarrow products + Cl^- \tag{8}$$

$$\cdot O_2^-/h^+ + OTC \rightarrow products \tag{9}$$

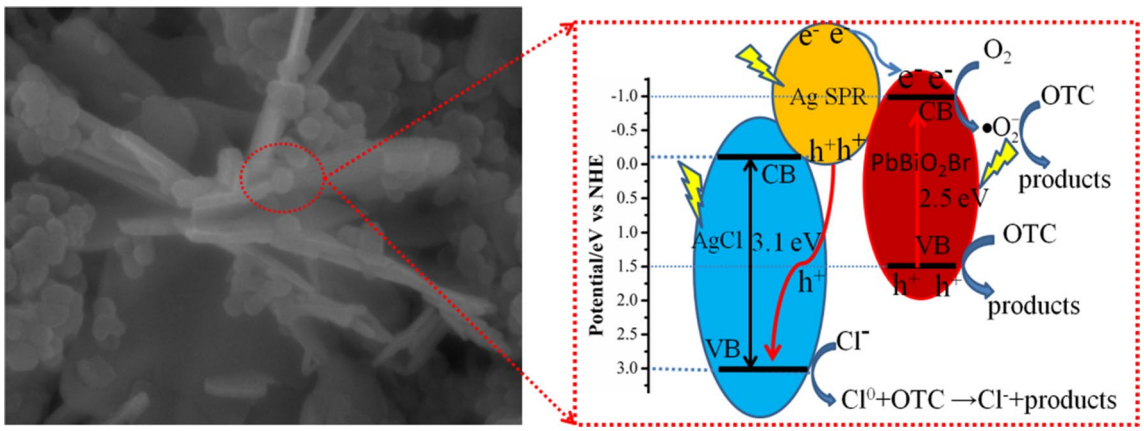

Fig. 7 Proposed photocatalytic reaction processes and charge separation of $Ag/AgCl/PbBiO_2Br$ composites under visible-light irradiation

4 Conclusions

In this study, visible-light-driven novel Ag/AgCl/$PbBiO_2Br$ composites were successfully synthesized through hydrothermal and in situ photoreaction method. The UV–Vis absorption spectra confirm that the as-obtained Ag/AgCl/$PbBiO_2Br$ composites exhibit remarkable photo-absorption property in the visible-light region as compared to $PbBiO_2Br$ nanosheets, which could be due to the surface Ag resonance. The Ag/AgCl/$PbBiO_2Br$ (20.4%) composite exhibits the strongest capacity for degradation of the antibiotic OTC under visible-light irradiation, which can be mainly attributed to strong visible-light absorbance and the efficiently separation of photoexcited charge. The recycling experiments demonstrate that the Ag/AgCl/$PbBiO_2Br$ composites possess good stability. In addition, active species trapping experiments confirm that $\cdot O_2^-$, Cl^0 and h^+ play an very important role in the degradation process. This work provides a way to design an excellent environmental purification material.

Funding This research has been supported by the China National Key R&D Project during the 13th Five-year Plan Period (Grant No. 2017YFB0602500) and University Natural Science Research Program of Jiangsu Province (16KJA610002).

Availability of data and materials All data are fully available without restriction.

Compliance with ethical standards

Conflict of interest The authors declare that they have no competing interests.

References

1. Q.J. Yu, T. Ouyang, K.F. Zhou, C.T. Chang, Photocatalytic degradation of oxytetracycline by photosensitive materials and toxicological analysis by caenorhabditis elegans. J. Nanosci. Nanotechnol. **19**, 6924–6932 (2019)
2. S.F. Wang, H.J. Gao, G. Sun, Y. Li, Y. Wang, H. Liu, C. Chen, L. Yang, Structure characterization, optical and photoluminescence properties of scheelite-type CaWO4 nanophosphors: effects of calcination temperature and carbon skeleton. Opt. Mater. **99**, 109562 (2020)
3. S.J. Jiao, S.R. Meng, D.Q. Yin, L.H. Wang, L.Y. Chen, Aqueous oxytetracycline degradation and the toxicity change of degradation compounds in photoirradiation process. J. Environ. Sci. **7**, 806–813 (2008)
4. Z.M. He, Y.M. Xia, B. Tang, J.B. Su, X.F. Jiang, Optimal co-catalytic effect of $NiFe_2O_4$/ZnO nanocomposites toward enhanced photodegradtion for dye MB. Z. Phys. Chem. **233**, 347–359 (2017)
5. E. Guine, J.A. Garrido, R.M. Rodriguez, P.L. Cabot, C. Arias, F. Centellas, E. Brillas, Degradation of the fluoroquinolone enrofloxacin by electrochemical advanced oxidation processes based on hydrogen peroxide electrogeneration. Electrochim. Acta. **55**, 2101–2115 (2010)
6. T. Xian, X.F. Sun, L.J. Di, Y.J. Zhou, J. Ma, H.Q. Li, H. Yang, Carbon quantum dots (CQDs) decorated Bi_2O_{3-x} hybrid photocatalysts with promising NIR-light-driven photodegradation activity for AO7. Catalysts **9**, 1031 (2019)
7. T. Xian, L.J. Di, X.F. Sun, H.Q. Li, Y.J. Zhou, H. Yang, Photo-Fenton degradation of AO7 and photocatalytic reduction of Cr(VI) over CQD-decorated $BiFeO_3$ nanoparticles under visible and NIR light irradiation. Nanoscale Res. Lett. **14**, 397 (2019)
8. Y.L. Yu, S.L. Huang, Y. Gu, S. Yan, Z.J. Lan, W.J. Zheng, Y.A. Cao, Study of $PbBiO_2X$ (X = Cl, Br and I) square nanoplates with efficient visible photocatalytic performance. Appl. Surf. Sci. **428**, 844–850 (2018)
9. F.Y. Liu, Y.R. Jiang, C.C. Chen, W.W. Lee, Novel synthesis of $PbBiO_2Cl$/BiOCl nanocomposite with enhanced visible-driven-light photocatalytic activity. Catal. Today **300**, 112–123 (2018)
10. B. Wang, J. Di, P.F. Zhang, J.X. Xia, S. Dai, H.M. Li, Ionic liquid-induced strategy for porous perovskite-like $PbBiO_2Br$photocatalysts with enhanced photocatalytic activity and mechanism insight. Appl. Catal. B **206**, 127–135 (2017)
11. B. Wang, J. Di, L. Lu, S.C. Yan, G.P. Liu, Y.Z. Ye, H.T. Li, W.S. Zhu, H.M. Li, J.X. Xia, Sacrificing ionic liquid-assisted anchoring of carbonized polymer dots on perovskite-like $pbBiO_2Br$ for robust CO_2 photoreduction. Appl. Catal. B **254**, 551–559 (2019)
12. F.Y. Xiao, J. Xing, L. Wu, Z.P. Chen, X.L. Wang, H.G. Yang, Assembly of ultrathin $PbBiO_2Br$ nanosheets with enhanced visible light photocatalytic properties. RSC Adv. **3**, 10687–10690 (2013)
13. C.K. Song, W.J. Feng, J.S. Zhao, X. Wang, Effect of drying temperature on properties of lithium-rich manganese-based materials in sol-gel method. Ionics **25**, 4607–4614 (2019)
14. M. Li, W. Feng, W. Su, X. Wang, Complex hollow structures of cobalt(II) sulfide as a cathode for lithium–sulfur batteries. Int. J. Electrochem. Sci. **15**, 526–534 (2020)
15. X. Li, J. Wang, D. Xu, Z. Sun, Q. Zhao, W. Peng, Y. Li, G. Zhang, F. Zhang, X. Fan, $NbSe_2$ nanosheet supported $PbBiO_2Br$ as a high performance photocatalyst for the visible light-driven asymmetric alkylation of aldehyde. ACS Sustain. Chem. Eng. **3**, 1017–1022 (2015)
16. S. Li, X. Wang, Y. Xu, H. Yang, F. Wei, X. Liu, The excellent photocatalytic synergism of $PbBiO_2Br$/UiO-66-NH_2 composites via multiple coupling effects. RSC Adv. **6**, 89907–89915 (2016)
17. Y.M. Xia, Z.M. He, J.B. Su, K.J. Hu, Construction of novel Cu_2O/$PbBiO_2Br$ composites with enhanced photocatalytic activity. J. Mater. Sci.: Mater Electron. **30**, 9843–9854 (2019)
18. Z.M. He, J.B. Su, R. Chen, B. Tang, Fabrication of novel p-Ag_2O/n-$PbBiO_2Br$ heterojunction photocatalysts with enhanced photocatalytic performance under visible-light irradiation. J. Mater. Sci.: Mater Electron. **30**, 20870–20880 (2019)
19. H.P. Lin, W.W. Lee, S.T. Huang, L.W. Chen, T.W. Yeh, J.Y. Fu, C.C. Chen, Controlled hydrothermal synthesis of $PbBiO_2Br$/BiOBr heterojunction with enhanced visible-driven-light photocatalytic activities. J. Mol. Catal. A **417**, 168–183 (2016)
20. M.J. Islam, D.A. Reddy, R. Ma, Y. Kim, T.K. Kim, Reduced-graphene-oxide-wrapped BiOI-AgI heterostructured nanocomposite as a high-performance photocatalyst for dye degradation under solar light irradiation. Solid State Sci. **61**, 32–39 (2016)
21. H.J. Gao, X.X. Zhao, H.M. Zhang, J.F. Chen, S.F. Wang, H. Yang, Construction of 2D/0D/2D face-to-face contact g-C_3N_4@Au@$Bi_4Ti_3O_{12}$ heterojunction photocatalysts for degradation of rhodamine B. J. Electron. Mater. (2020). https://doi.org/10.1007/s11664-020-08243-2
22. Z.H. Shah, Y.Z. Ge, W.Y. Ye, X.J. Lin, S.F. Zhang, R.W. Lu, Visible light activation of $SrTiO_3$ by loading Ag/AgX (X = Cl, Br) for

highly efficient plasmon-enhanced photocatalysis. Mater. Chem. Phys. **198**, 73–82 (2017)
23. D.B. Xu, W.D. Shi, C.J. Song, M. Chen, S.B. Yang, W.Q. Fan, B.Y. Chen, In-situ synthesis and enhanced photocatalytic activity of visible-light-driven plasmonic Ag/AgCl/$NaTaO_3$ nanocubes photocatalysts. Appl. Catal. B **191**, 28–234 (2016)
24. T.T. Sun, D.M. Cui, Q. Ma, X. Peng, L.J. Yuan, Synthesis of $BiVO_4$/MWCNT/Ag@AgCl composite with enhanced photocatalytic performance. J. Phys. Chem. Solids **111**, 190–198 (2017)
25. Z.M. He, J.B. Su, Y.M. Xia, B. Tang, Fabrication and photocatalytic performance of $Bi_{24}O_{31}Br_{10}$ nanosphere by a polyacrylamide gel method. Micro Nano Lett. (2020). https://doi.org/10.1049/mnl.2020.0016
26. J.B. Zhou, W. Liu, W.Q. Cai, The synergistic effect of Ag/AgCl@ZIF-8 modified g-C_3N_4 composite and peroxymonosulfate for the enhanced visible-light photocatalytic degradation of levofloxacin. Sci. Total Environ. **696**, 133962 (2019)
27. Y.F. Wang, M. Zhang, J. Li, H.C. Yang, J. Gao, G. He, Z.Q. Sun, Construction of Ag@AgCl decorated TiO_2 nanorod array film with optimized photoelectrochemical and photocatalytic performance. Appl. Surf. Sci. **476**, 84–93 (2019)
28. Y.X. Yan, H. Yang, Z. Yi, T. Xian, R.S. Li, X.X. Wang, Construction of Ag_2S@$CaTiO_3$ heterojunction photocatalysts for enhanced photocatalytic degradation of dyes. Desalin. Water Treat. **170**, 349–360 (2019)
29. Y.M. Xia, Z.M. He, J.B. Su, K.J. Hu, Polyacrylamide gel synthesis and photocatalytic performanceof $PbBiO_2Br$ nanosheets. Mater. Lett. **241**, 64–67 (2019)
30. Z.M. He, J.B. Su, B. Tang, Y.M. Xia, Fabrication of novel Cu_2O/$Bi_{24}O_{31}Br_10$ composites and excellent photocatalytic performance. J. Mater. Sci.: Mater Electron. **29**, 19544–19553 (2018)
31. Z.M. He, Y.M. Xia, J.B. Su, Fabrication of novel AgBr/$Bi_{24}O_{31}Br_10$ composites with excellent photocatalytic performance. RSC Adv. **8**, 39187–39196 (2018)
32. N.M. Mahmoodi, A. Taghizadeh, M. Taghizadeh, J. Abdi, In situ deposition of Ag/AgCl on the surface of magnetic metal-organic framework nanocomposite and its application for the visible-light photocatalytic degradation of Rhodamine dye. J. Hazard. Mater. **378**, 120741 (2019)
33. M.M. Sajid, N.A. Shad, A.M. Afzal, Y. Javed, S.B. Khan, N. Amin, A. Shah, I. Yousaf, H.F. Zhai, Generation of strong oxidizing radicals from plate-like morphology of $BiVO_4$ for the fast degradation of crystal violet dye under visible light. Appl. Phys. A **126**, 314 (2020)
34. Y.M. Xia, J.B. Su, Z.M. He, Z-scheme charge separation in $Bi_{24}O_{31}Br_{10}$/$SrTiO_3$ nanocomposites for degradation of methyl orange. J. Electron. Mater. **48**, 3890–3899 (2019)
35. Y.X. Yan, H. Yang, Z. Yi, X.X. Wang, R.S. Li, T. Xian, Evolution of Bi nanowires from BiOBr nanoplates through a $NaBH_4$ reduction method with enhanced photodegradation performance. Environ. Eng. Sci. **37**, 64–77 (2020)
36. Y.M. Xia, Z.M. He, W. Yang, B. Tang, Y.L. Lu, K.J. Hu, J.B. Su, X.P. Li, Effective charge separation in BiOI/Cu_2O composites with enhanced photocatalytic activity. Mater. Res. Express **5**, 025504 (2018)
37. Y.M. Xia, Z.M. He, J.B. Su, B. Tang, K.J. Hu, Y.L. Lu, X.P. Li, Fabrication of n-$SrTiO_3$/p-Cu_2O heterojunction composites with enhanced photocatalytic performance. J. Alloys Compd. **753**, 356–363 (2018)
38. M. Zhao, W. Zhou, M.M. Lu, Z.P. Guo, C.D. Li, W.J. Wang, Novel AgCl nanotubes/BiOCl nanosheets composite with improved adsorption capacity and photocatalytic performance. J. Alloys Compd. **773**, 1146–1153 (2019)
39. Y.M. Xia, Z.M. He, J.B. Su, One-step construction of novel Ag_3PO_4/$PbBiO_2Br$ composite with enhanced photocatalytic activity. Mater. Res. Express **6**, 085909 (2019)
40. M. Golkari, H. Shokrollahi, H. Yang, The influence of Eu cations on improving the magnetic properties and promoting the Ce solubility in the Eu Ce-substituted garnet synthesized by the solid state route. Ceram. Int. **46**, 8553–8560 (2020)
41. C.D. Yu, P. Wang, X.F. Wang, F. Chen, H.G. Yu, Silver-melamine nanowire-assisted synthesis of net-like AgCl-Ag/g-C_3N_4 for highly efficient photocatalytic degradation ability. J. Alloys Compd. **806**, 263–271 (2019)
42. S.F. Yang, C.G. Niu, D.W. Huang, H. Zhang, C. Liang, G.M. Zeng, $SrTiO_3$ nanocubes decorated with Ag/AgCl nanoparticles as photocatalysts with enhanced visible-light photocatalytic activity towards the degradation of dyes, phenol and bisphenol A. Environ. Sci-Nano **4**, 585–595 (2017)
43. J.W. Pan, Z.M. He, J.B. Su, R. Chen, B. Tang, Preparation and optical properties of Ni-doped $PbBiO_2Br$ nanoparticles. Mater. Res. Express **6**, 115042 (2019)
44. Y.M. Xia, Z.M. He, J.B. Su, X.P. Li, B. Tang, One-step construction of novel $PbBiO_2Br$/ZnO heterojunction composites with enhanced photocatalytic activity. Phys. Status Solidi A **216**, 1900406 (2019)
45. Y.M. Xia, Z.M. He, J.B. Su, S.Q. Zhu, B. Tang, Sustainable solar-light-driven $SrTiO_3$/$PbBiO_2Br$ nanocomposites with enhanced photocatalytic activity. J. Electron. Mater. **249**, 3259–3268 (2020)
46. O. Dehghani Dastjerdi, H. Shokrollahi, H. Yang, The enhancement of the Ce-solubility limit and saturation magnetization in the $Ce_{0.25}Bi_xPrY_{2.75-x-y}Fe_5O_{12}$ garnet synthesized by the conventional ceramic method. Ceram. Int. **46**, 2709–2723 (2020)
47. M.M. Sajid, N. Amin, N.A. Shad, S.B. Khan, Y. Javed, Z.J. Zhang, Hydrothermal fabrication of monoclinic bismuth vanadate (m-$BiVO_4$) nanoparticles for photocatalytic degradation of toxic organic dyes. Mater. Sci. Eng. B **242**, 83–89 (2019)
48. M.M. Sajid, N.A. Shad, A.M. Afzal, Y. Javed, S.B. Khan, Z. Imran, S. Hassan, Z. Hussain, Z.J. Zhang, N. Amin, Fast surface charge transfer with reduced band gap energy of $FeVO_4$/graphene nanocomposite and study of its electrochemical property and enhanced photocatalytic activity. Arab. J. Sci. Eng. **44**, 6659–6667 (2019)
49. M.M. Sajid, N.A. Shad, Y. Javed, S.B. Khan, Z.J. Zhang, N. Amin, H.F. Zhai, Preparation and characterization of Vanadium pentoxide (V_2O_5) for photocatalytic degradation of monoazo and diazo dyes. Surf. Interfaces **19**, 100502 (2020)
50. Z.M. He, Y.M. Xi, J.B. Su, B. Tang, Fabrication of magnetically separable $NiFe_2O_4$/$Bi_{24}O_{31}Br_{10}$ nanocomposites and excellent photocatalytic performance under visible light irradiation. Opt. Mater. **88**, 195–203 (2019)
51. C.X. Zheng, H. Yang, Z.M. Cui, H.M. Zhang, X.X. Wang, A novel $Bi_4Ti_3O_{12}$/Ag_3PO_4 heterojunction photocatalyst with enhanced photocatalytic performance. Nanoscale Res. Lett. **12**, 608 (2017)
52. Y.M. Xia, Z.M. He, J.B. Su, B. Tang, K.J. Hu, Y.L. Lu, S.P. Sun, X.P. Li, Fabrication of magnetically separable $NiFe_2O_4$/BiOI nanocomposites with enhanced photocatalytic performance under visible-light irradiation. RSC Adv. **8**, 4284–4294 (2018)
53. G.J. Gao, W.J. Feng, W.X. Su, S.J. Wang, L.J. Chen, M.M. Li, C.K. Song, Preparation and modification of MIL-101(Cr) metal organic framework and its application in lithium-sulfur batteries. Int. J. Electrochem. Sci. **15**, 1426–1436 (2020)
54. S.F. Wang, H.J. Gao, C. Chen, Q. Li, C. Li, Y. Wei, L. Fang, Effect of phase transition on optical and photoluminescence properties of nano-$MgWO_4$ phosphor prepared by a gamma-ray irradiation assisted polyacrylamide gel method. J. Mater. Sci.: Mater. Electron. **30**, 15744–15753 (2019)
55. K.H. Wu, Y.C. Cheng, K.F. Cheng, J.C. Wang, Antibacterial activity of surface-modified fabric with Ag/AgCl-doped quaternary a mmonium modified silicate hybrid. J Nanosci Nanotechnol. **19**, 7285–7293 (2019)

56. Q. Xiao, Z.C. Si, J. Zhang, C. Xiao, X.K. Tan, Photoinduced hydroxyl radical and photocatalytic activity of samarium-doped TiO_2 nanocrystalline. J. Hazard. Mater. **150**, 62–67 (2008)
57. S.F. Wang, C. Chen, Y. Li, Q. Zhang, H. Gao, Synergistic effects of optical and photoluminescence properties, charge transfer, and photocatalytic activity in $MgAl_2O_4$: Ce and Mn-codoped $MgAl_2O_4$: Ce phosphors. J. Electron. Mater. **48**, 6675–6685 (2019)
58. Y.M. Xia, Z.M. He, J.B. Su, Y. Liu, B. Tang, Fabrication and photocatalytic property of novel $SrTiO_3/Bi_5O_7I$ nanocomposites. Nanoscale Res. Lett. **13**, 148 (2018)
59. Z.M. He, Y.M. Xia, B. Tang, J.B. Su, Fabrication and photocatalytic property of magnetic $NiFe_2O_4/Cu_2O$ composites. Mater. Res. Express. **4**, 095501 (2017)
60. Y.M. Xia, Z.M. He, J.B. Su, B. Tang, Y. Liu, Enhanced photocatalytic performance of Z-scheme Cu_2O/Bi_5O_7I nanocomposites. J. Mater. Sci.: Mater. Electron. **29**, 15271–15281 (2018)
61. M. Li, W.J. Feng, W. Su, X. Wang, CoNi-embedded nitrogen-enriched porous carbon framework for long-life lithium–sulfur batteries. J. Solid State Electrochem. **23**, 2317–2324 (2019)
62. Y.M. Xia, Z.M. He, J.B. Su, B. Tang, Y. Liu, X.P. Li, Fabrication of novel n-$SrTiO_3$/p-BiOI heterojunction for degradation of crystal violet under simulated solar light irradiation. NANO **13**, 1850070 (2018)
63. X.X. Yao, X.H. Liu, D. Zhu, C.B. Zhao, L.D. Lu, Synthesis of cube-like Ag/AgCl plasmonic photocatalyst with enhanced visible light photocatalytic activity. Catal. Commun. **59**, 151–155 (2015)
64. Z.M. He, Y.M. Xia, B. Tang, X.F. Jiang, J.B. Su, Fabrication and photocatalytic property of ZnO/Cu_2O core-shell nanocomposites. Mater. Lett. **184**, 148–151 (2016)
65. S.F. Wang, H.J. Gao, Y. Wang, G. Sun, X. Zhao, H. Liu, C. Chen, L. Yang, Effect of the sintering process on the structure, colorimetric, optical and photoluminescence properties of $SrWO_4$ phosphor powders. J. Electron. Mater. (2020). https://doi.org/10.1007/s11664-020-07941-1
66. S.F. Wang, H.J. Gao, Y. Wei, Y.W. Li, X.H. Yang, L.M. Fang, L. Lei, Insight into the optical, color, photoluminescence properties, and photocatalytic activity of the N-O and C-O functional groups decorating spinel type magnesium aluminate. CrystEngComm **21**, 263–277 (2019)
67. Y.M. Xia, Z.M. He, Y.L. Lu, B. Tang, S.P. Sun, J.B. Su, X.P. Li, Fabrication and photocatalytic property of magnetic $SrTiO_3$/$NiFe_2O_4$ heterojunction nanocomposites. RSC Adv. **8**, 5441–5450 (2018)
68. M.M. Sajid, N.A. Shad, Y. Javed, S.B. Khan, N. Amin, Z.J. Zhang, Z. Imran, M.I. Yousuf, Facile synthesis of $Zn_3(VO_4)_2/FeVO_4$ heterojunction and study on its photocatalytic and electrochemical properties. Appl. Nanosci. (2018). https://doi.org/10.1007/s13204-019-01199-8
69. M.M. Sajid, N.A. Shad, Y. Javed, S.B. Khan, Z.J. Zhang, N. Amin, N. Amin, H.F. Zhai, Morphological effects on the photocatalytic performance of $FeVO_4$ nanocomposite. Nano-Struct. Nano-Object. **22**, 100431 (2020)